ISSN 2394-3777 (Print)
ISSN 2394-3785 (Online)
Available online at www.ijartet.com

International Journal of Advanced Research Trends in Engineering and Technology (IJARTET)
Vol. 4, Special Issue 4, March 2017

Optic Nerve Head Segmantaion – Tracking Photographs

N. Kokila,
Junior Assistant in Thiruvalluvar University College of Arts And Science,
Arakkonam.

Abstract—**Reliable and efficient optic nerve head segmentation is important tasks in automated retinal viewing. In a prescreening setting, special constraints are put on a system such as the one explained in this paper. The system should be completely automatic without any required user interaction as it should be able to set process large amounts of images. As the data in large-scale screening programs comes from various positions and is acquired by different operators with different equipment, there exists a large inconsistency in the image realization procedure. The global terms in the cost function are based on the orientation and width of the vascular pattern in the image, the general direction of retinal vessels at any given position in the image, a geometrical parametric model was proposed, Segmentation of the connective tissues in this area is essential to obtain an accurate measurement of arithmetical parameters and to build mechanical models. The structure tensor is used to characterize the predominant structure direction and the spatial coherence at each point, the natural lack of correspondence in the appearance of the retina and the fact that these images can be from a left or right eye and centered on different parts of the retina, it is clear that automatic segmentation is a challenging task. Automatic retinal image analysis can be complicated by the being there of pathology. Inconsistent image contrast or missing edge feature.**

Keywords— Active contours, optic nerve head, Image segmentation, screening, Photo tracking, Introduction.

I. INTRODUCTION

THIS paper presents an algorithm for the repeated localization and segmentation of the optic nerve head in retinal images. No user involvement is essential: the algorithm automatically selects the general location of the center of optic nerve head, then fits a contour to the optic nerve head rim. Localization is accomplishby means of a simple but valuable specialized strain; segmentation by fitting an active contour to the optic nerve head rim using a specialized three phase global and local deformable model that exploits the specific characteristics of the optic nerve head's appearance. We evaluate the algorithm against alternative approaches using a set of 100 random images drawn from diabetic screening programs, and present the results. In particular, the progress of disease and its response to treatment require the tracking of changes in retinal thickness along a given locus over.

Manuscript received February 2, 2004. This work was supported by the James Lowell, Andrew Hunter*, David Steel, AnsuBasu, Robert Ryder, Eric Fletcher, and Lee Kennedy.

In a prescreening setting, special requirements are put on a system such as the one described in this paper. The system should be completely automatic without any required user interaction as it should be able to batch process large amount of images. As the data in large-scale screening programs comes from multiple locations and is acquired by different operators with different equipment, there exists a large variability in the image acquisition process. Add to this the natural variation in the appearance of the retina and the fact that these images can be from a left or right eye and centered on different parts of the retina, it is clear that automatic segmentation is a challenging task.

Optic nerve head segmentation is a necessary step in this structured analysis for a number of reasons. First, the optic nerve head can itself act as a distractor: it is a large bright region thatcan be mistaken (by algorithms) for gross circulate exudation;the high-contrast rim also causes false responses to linear bloodvessel filters. Second, the vessels radiate from the optic nerve head, so vessel tracking algorithms may start from there.

Third, the optic nerve head is important in localization of the fovea, the central part of the retina that subserves fine vision. This lies at the center of a larger area, the macula. Retinopathy in this area, maculopathy, is associated with a high risk of visual loss. The macular is a dark approximately circular area, but the contrast is often quite small, and it may be obscured by exudates or blurring. Consequently a global correlational search often fails. The fovea is located approximately 2.5 disc diameters temporal to the temporal edge of the optic disc and between the major temporal retinal vascular arcades. These positional constraints can be used to identify a small search area for the macular, and to estimate the position if the search

ISSN 2394-3777 (Print)
ISSN 2394-3785 (Online)
Available online at www.ijartet.com

International Journal of Advanced Research Trends in Engineering and Technology (IJARTET)
Vol. 4, Special Issue 4, March 2017

fails, although variation in the optic disk size compromises the reliability of this method.

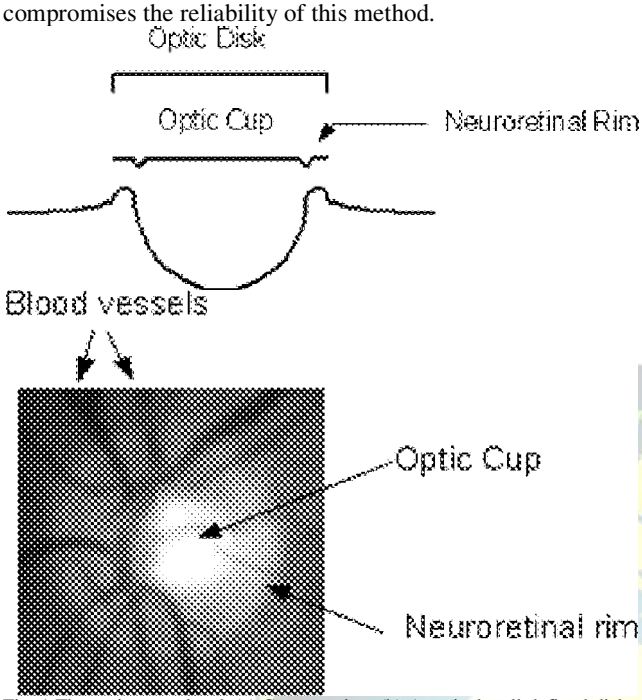

Fig. 1.The optic nerve head. (a) Cross section. (b) A typical well-defined disk

II. Optic Nerve Head

A. *Optic Nerve Head Appearance*

Successful segmentation of the optic nerve head requires a careful analysis of its appearance (see Fig. 1). It is the extremity of the optic nerve in the interior of the eye, and also the entrance and exit site of the retinal vessels [14]. The shape is approximately elliptical, with a vertical principal axis (width mm, height mm) [15]. As the nerve fibers reach the optic nerve head they turn and exit through the optic nerve, leaving a small depression (the "cup") in the center of the nerve head. There is often a brighter central region, the "pallor," which if present usually includes the cup. The optic disc rim is judged to be the inner margin of the peripapillary scleral ring, seen as a thin white band encircling the optic disc. In fundal images, the appearance varies quite substantially. The size and shape may vary significantly. The rim is usually visible as a bright boundary; the nasal side is usually less bright than the temporal side, and sometimes not visible at all. In some images, the entire optic nerve head is brighter than the surrounding area, so that it appears as a disk; in others the appearance is of a hollow ring. In either case the pallor may appear as a smaller, brighter disk within the optic disk. There may also be bright areas just outside the rim caused by peripapillary atrophy, either distorting the shape or forming concentric elliptical arcs. To complicate the issue further, departing vessels partially obscure the rim. The majorities climbs out on the nasal size and depart vertically; a smaller number depart nasally, with only a few fine vessels on the temporal side. Sometimes vessels turn at the nasal rim edge and run vertically, obscuring portions of the rim. A consequence of the nasal distribution of vessels is that the pallor, if visible, is mainly located to the temporal side. The variability in appearance misleads obvious approaches. Large areas of circulated exudates, which have high contrast, act as strong distracters for correlation-based localization algorithms—algorithms that work well on images of healthy retina may fail on a screening population. Similar problems

TABLE I
VISUAL CHARACTERISTICS

Characteristic	No. images
No detectable optic nerve head	4
Severe Cataract	8
Moderate Cataract	2
Total potentially unusable	10
Exudates or laser scars	7
Light artifacts	7
Easily visible choroidal vessels	20
Total localization endangered	34
Some of rim blurred or missing	27
Severe peripapillary atrophy	6
Moderate peripapillary atrophy	19
Concentric peripapillary atrophy/artifacts	23
Strong pallor distractor	13
Total segmentation endangered	58

B. *Screening Data*

We have tested the algorithms using a random sample of 100 fundal images taken from 50 patients attending the diabetic retinal-screening programme at City Hospital, Birmingham. Some of the patients had been referred from family practitioners, and consequently demographic data was unavailable for two. The mean age of the remaining patients was 63.7 years (s.d. 14.8 years), with 65.5% male and 34.5% female. The patients were from various ethnic backgrounds (Asian 20%, Afro-Caribbean 16%, Caucasian 50%, Unknown 14%). 19 patients had type 2 diabetes mellitus, while the diabetes status was unavailable for the remaining 31. Given the characteristics of the regional diabetic population, type 2 diabetes mellitus is likely to predominate in this group too. The images were acquired using a Canon CR6 45MNf fundus camera, with a field angle lens of 45, resolution 640 480. Images were converted to grey-scale by extracting the Intensity component from the HSI representation. There is considerable variation in the images, with many characteristics that can affect the algorithms; these are summarized in Table I

ISSN 2394-3777 (Print)
ISSN 2394-3785 (Online)
Available online at www.ijartet.com

International Journal of Advanced Research Trends in Engineering and Technology (IJARTET)
Vol. 4, Special Issue 4, March 2017

III. OPTIMIZATION

The cost function must be minimized to find the which best fits to an image. This can be done in the parameter space of the PDM or by directly moving the points that make up in the image. To obtain the best results, a combination of the two approaches is proposed. In the parameter space a general optimization method is used to find the combination of model parameters which generates whichminimizes. As exhibits many local minima this is not a trivial problem. Two standard optimization techniques were tested, simulated annealing (SA) [16], [17] and Powell's optimization method [18]. Given enough running timeSA is guaranteed to find the global minimum. However, thisproperty in combination with the large number of model parametersmakes it a slow algorithm. A local optimization methodsuch as Powell is not guaranteed to find a global minimum butconverges towards a local minimum quickly. It was found thatusing a combination of global and local optimization methodscoupled to an image space optimization gave good performancein combination with an acceptable running time of the algorithm.The proposed optimization method can be divided intothree steps; first parameter space optimization, image space optimizationand second parameter space optimization.

A. Parameter Space Optimization:

The optimization procedure starts by performing a SA optimization of the four major modes of the PDM. These modes contain most of the major model pose variations such as rotation, translation, and scaling. In this way the model can roughly find the correct position in the image. This can be thought of as finding a good initialization, which is very important for the image space optimization step.

B. Validation Using an Artificial Dataset

The lack of ground truth segmentations for the ONH datasets Complicates the task of validating the described algorithms. Manual tracing, which in this case represents a particularly tedious and time-consuming process, was difficult due to the 3-D complexity of the structures involved, combined with the artifacts that appear in the 3-D datasets. Manual segmentation was deemed to lack the 3-D coherence present in the original structures that is necessary for generating biomechanical models. The possibility of using manual segmentation as ground truth for the segmentation algorithm was, thus, discarded. Instead we used artificial datasets, generated in a way that mimics the characteristics of the ONH datasets

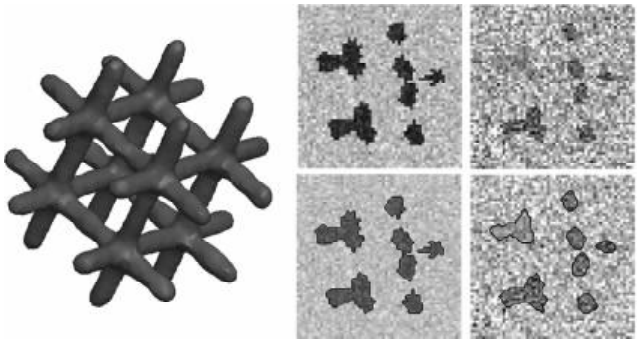

The process used in artificial validation dataset generation is as follows

- Generation of the initial 3-D dataset containing 12 orthogonal cylindrical beams with predetermined diametersthat simulate the connective tissue meshwork. A 3-D rendering is shown in Fig. 3.
- Calculation of binary images corresponding to parallel slices of the dataset acquired in an arbitrary plane orientation.
- Elimination of beam areas at random locations. At these locations, the beam area identified in the section isdeleted.
- Assignment of intensity values to beam/background voxel classes in the images. Values were selected randomly following two Gaussian distributions.
- Introduction of intersection illumination variations, by means of error factors that multiply the image intensity values.

C. A Clustering Alforithm

Since the intensity of the optic disk is much higher than the retinal background, a possible method in order to localize the optic disk is to find the largest clusters of pixels with the highest gray levels. For this reason, the pixels with the highest 1% gray levels are selected. After this, a clustering algorithm groups the nearby pixels into clusters. Initially, each point is a cluster and its own centroid.If the Euclidean distance between two centroids is less than a specified threshold ε, these clusters are combined to form a new one. The new centroid (c_x, c_y) is computed by means of Equations 1 and 2.

$$c_x = \sum_{i=0}^{n} x_i/n \quad \ldots\ldots\ldots \quad (1)$$

$$c_y = \sum_{i=0}^{n} y_i/n \quad \ldots\ldots\ldots \quad (1)$$

ISSN 2394-3777 (Print)
ISSN 2394-3785 (Online)
Available online at www.ijartet.com

International Journal of Advanced Research Trends in Engineering and Technology (IJARTET)
Vol. 4, Special Issue 4, March 2017

$i=0$

where(x_i, y_i) are the cluster points and n is the number of points in the cluster. If there are bright areas as well as the optic disk in the retinal image, the algorithm might compute several clusters.

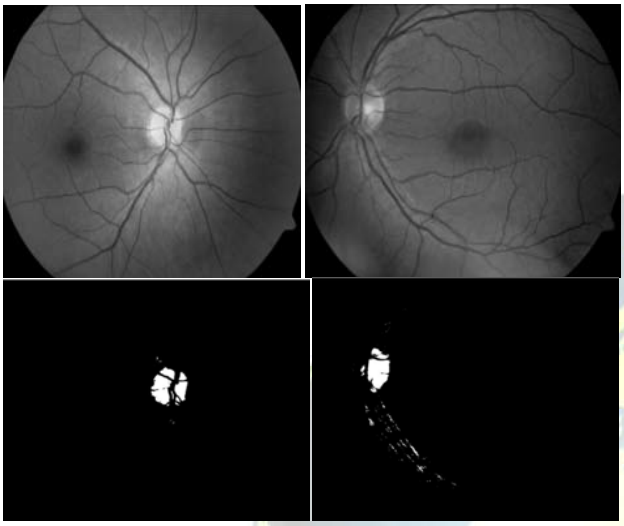

D. Testing and Results

We tested our algorithm against a number of alternative approaches, describe below. We used a subset of 90 images, excluding those with no discernable optic disk, or with severe Cataracts to prevent meaningful segmentation. To produce a "gold standard" segmentation four clinicians manually delimited the rim; we calculate their mean contours, and the radial standard deviations of these contours.

A. Parameter Settings

We experimented with a wide range of parameter settings, Including: initial model diameter and aspect ratio, Gaussian

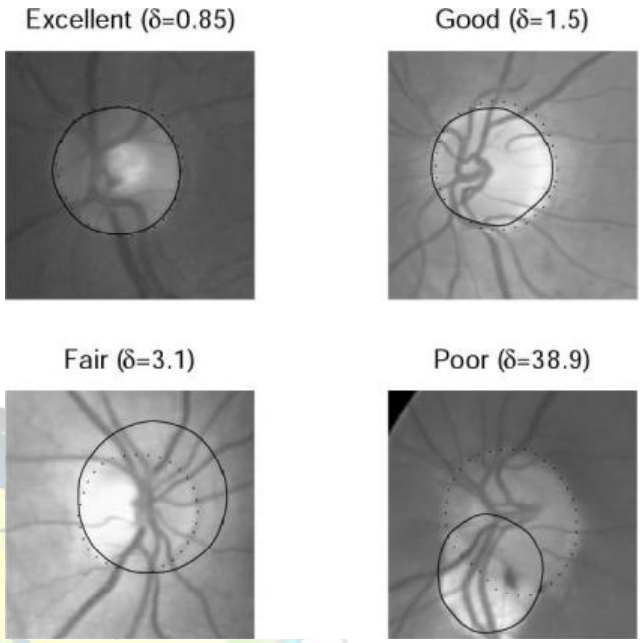

Fig. 6. Sample Segmentations. (a) Excellent. (b) Good. (c) Fair. (d) Poor. Solid
line: algorithm; dotted line: mean clinician boundary.

TABLE III
SUBJECTIVE CLASSIFICATION OF PERFORMANCE

(%)	*Excellent*	*Good*	*Fair*	*Poor*
TemporalLock	42	31	10	17
Simple	9	8	30	53
DV − Hough	39	22	20	19

Smoothing factors, radial profile search sizes, and in the deformable model.

B. Performance of the Algorithm

Fig. 7(a) shows the performance graph of our final algorithm against a simple benchmark approach ("direct") which proceeds directly from localization to local fitting without using the temporal lock or the vector gradient. Qualitatively, we define four categories (Excellent, Good, Fair, and Poor) containing images with disparity up to one, two, five, or more, respectively. Fig. 6 shows examples in each category. Table III summarizes performance on this subjective scale.

ISSN 2394-3777 (Print)
ISSN 2394-3785 (Online)
Available online at www.ijartet.com

International Journal of Advanced Research Trends in Engineering and Technology (IJARTET)
Vol. 4, Special Issue 4, March 2017

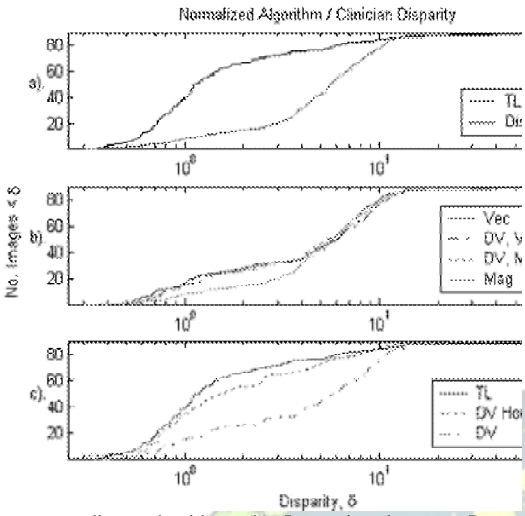

Fig. 7. (a) TL versus direct algorithm. (b) Interaction between De-vascularization (DV) and vector (Vec)/magnitude (Mag) gradient versions of direct algorithm. (c) Temporal Lock (TL), De-vascularized Hough (DV Hough), and De-vascularized direct (DV).

IV. System Description

The system operation divides into two parts, an *adaptive* phase and an *operational* phase, each outlined below. *Adaptive Phase:* The nerve head is first identified in each video field using a multistage, fairly computationally expensive process (Hough transform, dual eigenspace projection, geometric consistency check). The detected nerve head position serves as a fiducial reference to co-register all video fields processed during adaption, each of which has been filtered to enhance blood vessel structures. These registered, enhanced images are accumulated into a vascular distribution model for that particular subject. Errors in this stage are infrequent, but more Importantly, the errors are incoherent. That is, frequent correct Detections of the nerve head lead to aligned vascular structuresin the accumulated model, while infrequent erroneous detections lead to vascular structures randomly distributed over the model.

Adaptive Phase Outline.

• Image preparation:

— separate into fields, downsample;

— SLD spot detect, mask;

— filter to enhance retinal structures (vessels, nerve head Perimeter).

• Nerve head detection:

— detect retinal structures;

— Hough transforms circle extraction from retinal structures;

— Dualeigenspace projection to evaluate circle neighborhoods;

— Geometric consistency analysis of best nerve head candidates;

• Register vessel contour images and accumulate vascular Distribution model.

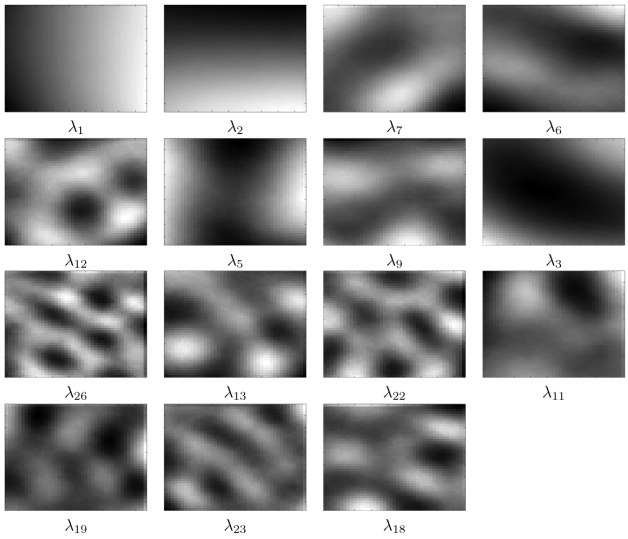

A. Operational Phase:

Each incoming vessel-enhanced image is cross correlated with the vascular distribution model constructed in the adaptive phase to identify the current translation of the retina. This process involves only FFTs and simple peak-finding; it is, therefore, quite fast.

Operational phase outline:

• Image preparation (as in adaptive phase);

• FFT-based crosscorrelation with vascular distributionmodel;

• identify peak and report relative translation.

B. Adaption: Detecting Retinal Structures

Once the incoming frames are separated into fields and sub sampled, and the SLD's spot(s) masked, we condition the images with the minimum filter described in [8] to dilate the vessel profiles and give them more uniformly dark interiors. Each video field is then filtered using the pair of 1-D templates shown in Fig. 9; the difference in horizontal and vertical filter length accommodates the dominant vertical orientation of the vasculature. These filters respond to blood vessels with a positive-going peak flanked by a pair of negative-going pulses; they respond to the nerve head perimeter with a "doublet" of opposite-polarity pulses. In either case, local maxima in the response correspond to features of possible interest. We use these simple filters because they are fast, and they suffice. Our need is essentially

ISSN 2394-3777 (Print)
ISSN 2394-3785 (Online)
Available online at www.ijartet.com

International Journal of Advanced Research Trends in Engineering and Technology (IJARTET)
Vol. 4, Special Issue 4, March 2017

for single scale detection, and the image quality is limited so that more sophisticated approaches such as the Sarkar-Boyer operator [27] or that in [8] offers no advantage. The filter response to the masked SLD spots is a relatively weak, disorganized region of small peaks that is easily disregarded. We denote the filtered image

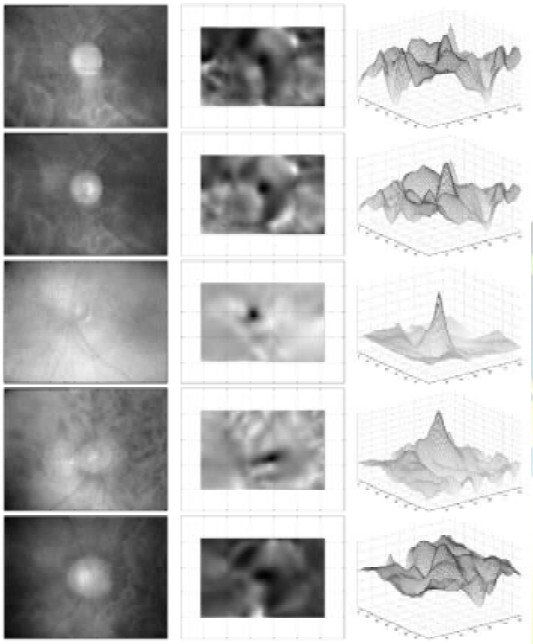

C. Related work

Our work differs from previous methods in that we use blood Vesselconvergences are the primary feature for detection.We test our method on 81 images showing a variety of retinal diseases, confusing lesions and manifestations. On this difficult data set, our method achieves an 89% correct detection rate.

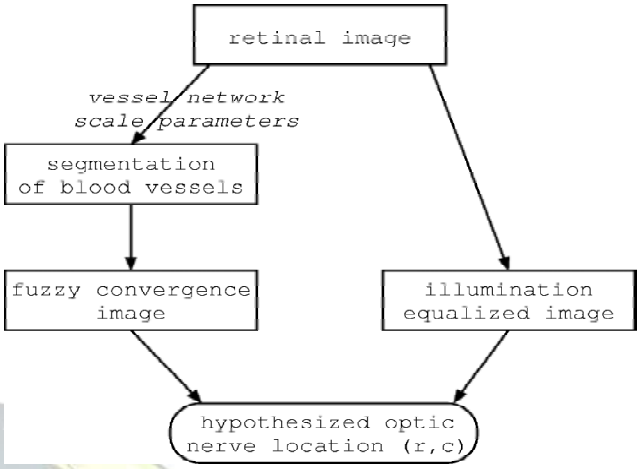

The system as implemented is not truly real-time, although the operational phase, being little more than a cross correlation, could easily be made to run in real time on appropriate hardware (e.g., a specialized DSP device). Ideally, of course, we would use the detected eye position to *steer* the SLD beam in real time such that the desired trajectory with respect to the retina was achieved even as the eye moved. The prototype system we have described contains the elements essential to such a development, but to do so would be a matter of considerable complexity and lies (well) beyond the scope of this work.

CONCLUSION

We have presented algorithms for localization and segmentation of the optic nerve head, an important stage in structured analysis of the retina, which can be used in diagnosis of eye diseases such as diabetic retinopathy. Although a number of methods have been published for optic Nerve head localization, many are unreliable when confronted With images of diseased retinue including strong distracters, and the reliable methods tend to be quite computationally complex. We have presented a simple but effective algorithm for localization optic Nerve Head Segmentation. In This Paper we conclude the overview of image process using eye diseases can complete localization.

Optic nerve head segmentation by active contours has not been extensively examined in the past. There are significant problems in dealing with distracters along blood vessels edges and the pallor, and with the very variable appearance of the optic nerve head. Previously published techniques require careful initialization of the model position, preprocessing of the image using morphological operations, and perform badly where the rim is faint or undetectable. In contrast, the algorithm presented in this paper exploits specific

ISSN 2394-3777 (Print)
ISSN 2394-3785 (Online)
Available online at www.ijartet.com

International Journal of Advanced Research Trends in Engineering and Technology (IJARTET)
Vol. 4, Special Issue 4, March 2017

features of the optic nerve head anatomy to achieve good localization while avoiding distracters. The temporal lock algorithm exploits the natural shape of the rim to bypass blood vessels and avoid the pallor, and the global and local deformable model deals effectively with weak areas of rim and vessel crossings. Defining energy functions and using a quasi-Newton optimization strategy makes the algorithm reasonably fast.

REFERENCES

1. A. Manivannan, P. F. Sharp, R. P. Phillips, and J. V. Forrester, "Digital fundus imaging using a scanning laser ophthalmoscope," *Physiol.Meas.*, vol. 14, pp. 43–56, 1993.
2. D. E. Singer, D.M. Nathan, H. A. Fogel, and A. P. Schachat, "Screening or diabetic retinopathy," *Ann. Int. Med.*, vol. 116, pp. 660–71, 1992.
3. J. J. Kanski, *Clinical Ophthalmology*, 3rd ed. London, U.K.: Butterworth- Heinemann, 1994.
4. E. M. Kohner, *Diabetes and the Eye, Oxford Textbook of Ophthalmology*. Oxford, U.K.: Oxford Univ. Press, 1999, vol. 2.
5. A. Hoover, V. Kouznetsova, and M. Goldbaum, "Locating blood vesselsin retinal images by piecewise threshold probing of a matched filter response,"*IEEE Trans. Med. Imag.*, vol. 19, pp. 203–210, Mar. 2000.
6. T. Teng, M. Lefley, and D. Claremont, "Progress toward automated diabetic ocular screening: A review of image analysis and intelligent systems for diabetic retinopathy," *Med. Biol. Eng, Comput.*, vol. 40, pp. 2–13, 2002.
7. A. Daxer, "Characterization of the neovascularization process in diabetic retinopathy by means of fractal geometry: Diagnostic implications,"Graefe's Arch. Clin. Exp. Ophthalmol., vol. 231, pp. 681–686, 1993.
8. W. Lotmar, A. Freiburghaus, and D. Bracher, "Measurement of vessel tortuosity on fundus photographs," Graefe's Arch. Clin. Exp.Ophthalmol., vol. 211, pp. 49–57, 1979.
9. P. H. Gregson, Z. Shen, R. C. Scott, and V. Kozousek, "Automated grading of venous beading," Comput. Biomed. Res., vol. 28, pp.291–304, 1995.
10. M. H. Goldbaum, V. Kouznetsova, B. L. Coté, W. E. Hart, and M. Nelson, "Automatic registration of digital ocular fundus images for comparison of lesions," in Proc. SPIE 1877, Ophthalmic Technologies III, 1995, pp. 291–304.
11. A. Can, C. Stewart, and B. Roysam, "Robust hierarchical algorithm for constructing a mosaic from images of the curved human retina," in *Proc. IEEE Computer Society Conf. Computer Vision and Pattern Recognition*, Fort Collins, CO, June 1999, pp. 286–292.
12. D. OttandW. Daunicht, "Eye movement measurement with the scanning laser ophthalmoscope," *Clin. Vis. Sci.*, vol. 7, pp. 551–556, 1992.
13. M. Kirby and L. Sirovich, "Application of the karhunen-loeve procedure for the characterization of human faces," *IEEE Trans. Pattern Anal. Machine Intell.*, vol. 12, pp. 103–108, Jan. 1990.
14. L. Sirovich and M. Kirby, "Low-dimensional procedure for the characterization of human faces," *J. Opt. Soc. Amer. A*, vol. 4, no. 3, pp. 519–524, Mar. 1987.
15. M. Turk and A. P. Pentland, "Eigenfaces for recognition," *CogNuero*, vol. 3, no. 1, pp. 71–96, 1991.
16. J. Zhang, Y. Yan, and M. Lades, "Face recognition: Eigenface, elastic matching, and neural nets," *Proc. IEEE*, vol. 85, pp. 1423–1435, Sept. 1997.
17. A. P. Pentland, B. Moghaddam, and T. Starner, "View-based and modular eigenspaces for face recognition," in *Vismod*, 1993.
18. S. Z. Li, "Face recognition based on nearest linear combinations," inProc. IEEE Computer Society Conf. Computer Vision and PatternRecognition, 1998, pp. 839–844.
19. S. Z. Li and J.Juwei Lu, "Face recognition based on nearest line method," IEEE Trans. Neural Networks, vol. 10, pp. 439–443, Mar.1999.
    T. F. Cootes, C. J. Taylor, D. H. Cooper, and J. Graham, "Active shape models—their training application," Comput. Vis. Image Understanding,vol. 61, no. 1, pp. 38–59, Jan. 1995.
20. James Lowell, Andrew Hunter*, David Steel, AnsuBasu, Robert Ryder, Eric Fletcher, and Lee Kennedy. IEEE Transactions on medical imaging vol 23 feb 2, 2004.